Non–enzymatic Amperometric Sensor for H₂O₂ Based on MnCO₃ Thin Film Electrodes

Sasho Stojkovikj,[1,]* Metodija Najdoski,[1] Birhan Sefer,[1,2] Valentin Mirčeski[1]

[1] Institute of Chemistry, Faculty of Natural Sciences and Mathematics, Ss. Cyril and Methodius University, Arhimedova 3, PO Box 162, 1000 Skopje, Republic of Macedonia

[2] Institute for Surface Science and Corrosion, Department of Materials Science and Engineering, Friedrich-Alexander-University of Erlangen-Nuremberg, D-91058 Erlangen, Germany

* Corresponding author's e-mail address: sashostojkovikj@gmail.com

Abstract: The present study describes development of a non–enzymatic amperometric sensor for detection of H₂O₂ based on MnCO₃ thin film electrodes. The film was deposited on electroconductive FTO coated glass substrates using simple chemical bath deposition method. The phase composition of the thin film was confirmed by X-ray diffraction analysis. The electrochemical properties and the sensor sensitivity towards H₂O₂ were examined using cyclic voltammetry and chronoamperometry in 0.1 M phosphate buffer solution with pH = 7.5. It was revealed that the sensing mechanism is based on electrocatalytic oxidation of H₂O₂, involving Mn species as redox mediators. According to the results, the best sensor response towards H₂O₂ was found at E = +0.25 V, with detection limit and sensor sensitivity of 10.0 μM and 2.64 μA cm^{-2} mM^{-1} (for the range of 0.09–1.8 mM), respectively, associated with R^2 = 0.999.

Keywords: amperometric sensors, hydrogen peroxide, manganese(II) carbonate thin films, electrocatalysis.

INTRODUCTION

THIS research contributes to the application of manganese(II) carbonate (MnCO₃), which already demonstrated interesting behaviour when used for preparing electrochromic materials,[1] as a precursor for synthesizing perovskites applied in high temperature solid oxide fuel cells,[2] and especially as an electrode material in supercapacitors.[3–7] The possibility of controlled deposition of uniform MnCO₃ thin films on FTO-coated substrates,[1] makes this material eligible to be studied as a working electrode in electrochemical systems for hydrogen peroxide (H₂O₂) sensor applications. H₂O₂ is an important substance that finds a wide use in various fields. Its oxidizing properties enable application in chemical and petro-chemical industry as a strong oxidizer, bleaching agent, disinfectant and propellant. [8–14] H₂O₂ is also used in medicine, pharmacy, cosmetics, food and beverage industry.[10,13–16] Apart from industrial applications, H₂O₂ is also important for the living cells.[17] It is well established that H₂O₂ is formed as a product in the mitochondria due to enzymatic reactions that involve free radicals.[17,18] Moreover, the increased mitochondrial production of H₂O₂ causes cytotoxic effects[11,13,18,19] through activation of several classes essential signalling proteins that compromise the cell reproduction, causing diseases such as cancer, diabetes, cardiovascular and neurodegenerative disorders.[17,20,21] The presence of H₂O₂ in the cells is significantly detrimental and commonly responsible for proliferation, apoptosis and/or necrosis of the cells, which depends on the cytosolic steady state concentration.[18,20] From this point of view, an accurate and precise quantification of H₂O₂ is substantially important. Hence, an enormous research strive is in progress in order to develop simple, efficient and reliable methods for detection and quantification of H₂O₂ at relatively low concentrations in biological fluids.[17] There are numerous methods for detection and quantification of H₂O₂. These include redox titrations,[22] chemiluminescence,[23–26] fluorescence and fluorimetry,[27–29] spectrophotometry,[30–32] chromatography[33] and electrochemistry.[13,34] The electrochemical sensors are based on sensing either reduction or oxidation

of H₂O₂ and they were shown to provide the most satisfactory level in terms of low detection limit, selectivity, simplicity and cost–effectiveness.[13,16,17,20,34] The electrochemical sensors can be either enzymatic or non-enzymatic types of sensors. The enzymatic electrochemical sensors are based on immobilization of enzymes on the sensor surface. Many scientists reported that these types of sensors are successful for detection of H₂O₂, showing relatively low detection limits, high sensitivity and selectivity.[35–40] Unfortunately, these sensors are facing with significant drawbacks such as instability, high costs due to use of expensive chemicals, complicated enzyme immobilization procedures, denaturation of enzymes, limited lifetime and poor reproducibility.[35–40] In contrast, the non-enzymatic electrochemical sensors based on transition elements that are simpler in design are proven to be reliable with high sensitivity and selectivity and quick response, suitable for detection in wide concentration range of the analyte and provide satisfactory low detection limits. These types of sensors usually include manganese oxides in form of nanosheets,[42,43] nanocomposites,[44–46] thin films,[16,47] nanoparticles,[16,48,49] nanowires,[20,50] nanofibers,[9] nanorods[51] and microspheres[15] combined with carbon nanotubes,[44,52–55] carbon nanofibers,[49] graphene,[20,53,56] graphene oxide,[12,54,57] ordered meso-porous carbon,[10] carbon foam,[42] carbon cloth,[8] etc.

The present paper demonstrates development of a novel, simple, non-expensive electrochemical and non-enzymatic amperometric sensor based on MnCO₃ thin film electrode for efficient selective detection and quantification of H₂O₂. The proposed H₂O₂ sensor is reliable, stable and robust even after being used for several dozens of times. Due to its relatively high detection limit towards H₂O₂ (10.0 µM), regrettably this sensor cannot find use as potential candidate for detecting H₂O₂ in biological systems. However, we are strongly encouraging its potential application for detecting H₂O₂ in the chemical, pharmaceutical and food and beverage industry and investigations in that direction are currently in progress by our research group.

EXPERIMENTAL SECTION

Commercially available fluorine doped tin oxide (FTO) coated glass substrates with dimensions of 20 × 3 mm and electric resistance of 10–20 Ω cm⁻² were used as working electrodes. The thin films of MnCO₃ were deposited using a previously described chemical bath deposition method (see Figure S1 from Supplementary material) where the thickness of the film is dependant from the deposition time, according to Figure 1.[1] The films were deposited with a thickness of 75, 100 and 150 nm. Phase identification of the synthesized MnCO₃ thin film was performed by Rigaku
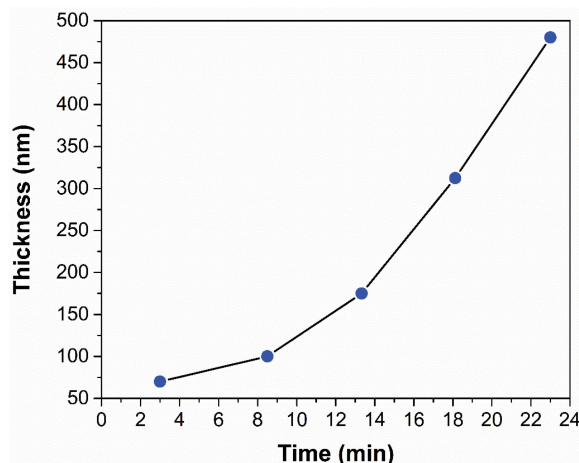

Figure 1. Thickness of the MnCO₃ films vs. deposition time.

Ultima IV X–Ray diffraction instrument. CuKα radiation was used in the 2ϑ range of 10°–70°. The electrochemical measurements were carried out using microAUTOLAB II potentiostat (Eco, Utrecht, Netherlands) and conventional three electrode system consisting of working electrode (MnCO₃ thin film deposited on FTO substrate), reference electrode (KCl saturated Ag/AgCl) and Pt wire as auxiliary electrode. Constant surface area on the working electrode was accomplished using silicone adhesive, heating glue gun and microscope slide (see Figure S2 from Supplementary material). This step was carried out to enable comparison of current density $-j/\mathrm{A\,cm^{-2}}$ values and prevent any interference of the electrode surface on the current density. Cyclic voltammetry and hydrodynamic chrono-amperometry were used for testing the sensing properties of the thin film modified electrodes towards H₂O₂. All electrochemical measurements were performed in a phosphate buffer solution - PBS (KH₂PO₄/K₂HPO₄) with c = 0.1 M and pH = 7.5. The pH of the buffer solutions was measured using pH-meter (model Voltcraft pH–100 ATC). The PBS was prepared using double distilled water with conductivity <5 µS cm⁻¹. The electrochemical measurements were carried out in a glass cell with 50 mL volume of PBS and under constant stirring of the electrolyte with 200 rpm. The H₂O₂ used for the electrochemical measurements was prepared always fresh through dilution of concentrated hydrogen peroxide solution (w = 25−30 %), and added in always freshly prepared PBS up to approximate concentration of 0.5 M. The exact concentration of H₂O₂ in the PBS stock solution was determined right before each electrochemical measurement through conventional permanganate titration method.[22] The electrochemical measurements were performed by injection of precise volume aliquots from the PBS stock solution into the electrochemical cell using micropipette. The following chemical compounds were

tested for possible interferences of the thin film modified electrodes with respect to H$_2$O$_2$: D-(+)-glucose, sodium citrate, potassium chloride and sodium nitrite. All electrochemical measurements were performed at room temperature in ambient conditions. All reagents used during the experiment were of analytical grade purity and purchased from Alkaloid AD - Skopje.

RESULTS

The phases of the thin films were identified using X–Ray Diffraction (XRD) analysis by separately recording diffractograms on the following samples: a) the precipitate from the chemical bath, b) the thin film deposited on a FTO coated substrate and c) the bare FTO coated substrate. Figure S3 (from Supplementary material) shows the recorded XRD patterns. The XRD patterns of the thin film deposited on the FTO coated substrate show a combination of patterns from both, the precipitate and the FTO layer (see Figure S3b from Supplementary material), respectively. Moreover, some of the patterns from both materials are overlapped (see Figure S3b from Supplementary material). The XRD results indicate that the thin film is chemically and structurally identical with the precipitate from the chemical bath and corresponds to well crystalized rhodochrosite phase manganese(II) carbonate (JCPDS 83–1763). In addition, it was also confirmed that the patterns of the FTO layer (see Figure S3c from Supplementary material) correspond to SnO$_2$ (JCPDS 46–1088).

The electrochemical measurements that were conducted by cyclic voltammetry were performed into four stages where all the examined MnCO$_3$ films were deposited with thickness of 75 nm, unless stated otherwise.

In the first stage, the possible electrochemical interference of the silicon adhesive used for providing constant surface area of the working electrode was tested if results in electrochemical response. The cyclic voltammetry was conducted on a completely covered FTO coated substrate (with the mentioned adhesive) and it was proved that the adhesive is not electroactive in the potential window from −1.0 to +1.5 V in the presence of H$_2$O$_2$ and in a PBS (see Figure S4 from Supplementary material).

In the second stage, the electrochemical response of H$_2$O$_2$ at the FTO layer was examined. Figure 2 shows repetitive cyclic volammograms of FTO electrode in the potential range of −1.0 to +1.5 V, in the absence and in the presence of H$_2$O$_2$ over the concentration interval from 0.05 to 5.0 mM, respectively. The voltammogram recorded in the absence of H$_2$O$_2$ shows a polarization curve of the FTO electrode in the PBS with a small reductive peak in the interval −0.6 to −1.0 V (Figure 2), for which is considered that is associated with the reduction of dissolved oxygen in the PBS. In the presence of H$_2$O$_2$, typical anodic and
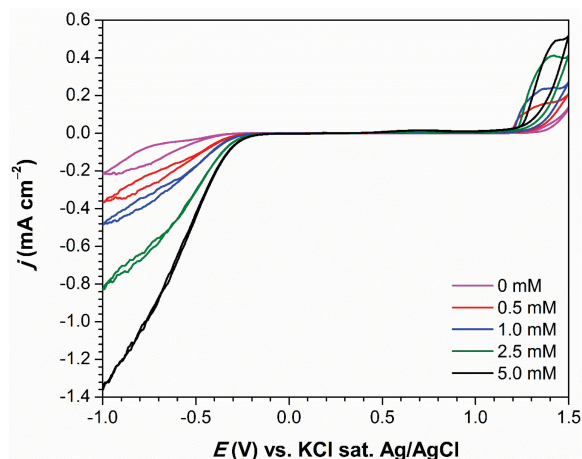

Figure 2. Repetitive cyclic voltammograms of FTO electrode in PBS (pH = 7.5) in absence of H$_2$O$_2$ and in presence of H$_2$O$_2$ with concentrations from 0.05–5.00 mM. Start potential: +1.5 V; 1st vertex potential: −1.0 V; 2nd vertex potential: +1.5 V. Scan rate: 5 mV s^{-1}.

cathodic processes take place, corresponding to the oxidation of H$_2$O$_2$ at potentials more positive than +1.20 V, and reduction at more negative potentials than −0.25 V (Figure 2). Obviously, the electrode reactions at bare FTO electrode are sluggish, requiring large overpotentials.

In the third stage, the electrochemical activity of the MnCO$_3$ thin film was examined. Figure 3 shows cyclic voltammograms of MnCO$_3$ thin film deposited on the FTO surface, in presence of H$_2$O$_2$ with different concentrations. The recorded voltammograms indicate that the MnCO$_3$ thin film manifests a complex electrocatalytic activity involving
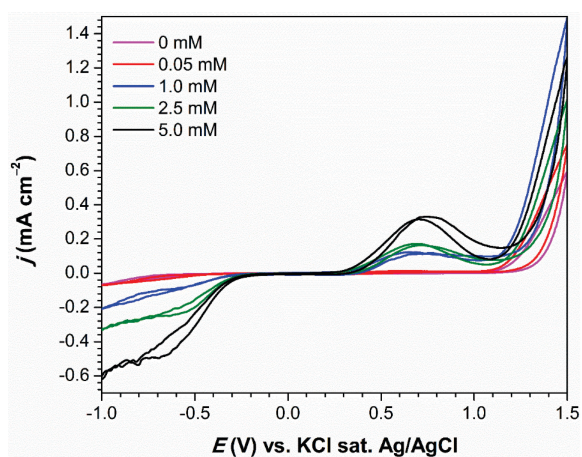

Figure 3. Typical cyclic voltammogram of FTO electrode covered with MnCO$_3$ thin film in PBS (pH = 7.5) in presence of H$_2$O$_2$ with concentrations from 0.05–5.00 mM. Start potential: +1.5 V; 1st vertex potential: −1.0 V; 2nd vertex potential: +1.5 V. Scan rate: 5 mV s^{-1}.

intricate redox reaction/s between polyvalent Mn species and H_2O_2. Thus, it is assumed that the sensing mechanism is most probably based on the interaction of the mentioned redox active species.

In the last fourth stage, the electrochemical activity of the $MnCO_3$ film in the presence of H_2O_2 at c = 5.0 mM, was investigated at different scan rates 1, 5, 10 and 20 mV s^{-1} (see Figure 4). Note that Figures 4a and 4b are separate set of cyclic voltammetry measurements carried out at the same experimental conditions, where the only difference is in the scanning direction in terms of the start potential. These experiments have been carried out in the potential range from +0.20 V to +1.25 V in order to focus only on the transformations where Mn species and H_2O_2 are involved, thereby avoiding the reduction of H_2O_2 at potentials bellow –0.25 V. It was discerned that the shape of the voltammograms is almost unaffected by the scan rate i.e. the trend remains the same. In addition, it was also discerned that the shapes of the voltammograms are not affected either by the starting potential of the cyclic voltammetry experiment. This is evidenced and concluded by comparison of the voltammograms shown in Figure 4a and 4b. The more positive starting potential of +1.20 V (see Figure 4a) and the less positive starting potential of +0.20 V (see Figure 4b) compared to the anodic peak potentials (see Table 1) did not influenced the shape of the recorded voltammograms.

The amperometric response of the sensor as a function of the H_2O_2 concentration was examined at potentials of +0.15, +0.20, +0.25 V in the concentration interval from 0.09 to 20.0 mM, aiming to find the optimal potential in order to maximize the detection limit, the linearity, the sensitivity and the response time. The cyclic voltammograms shown in Figure 3 indicate that the peak
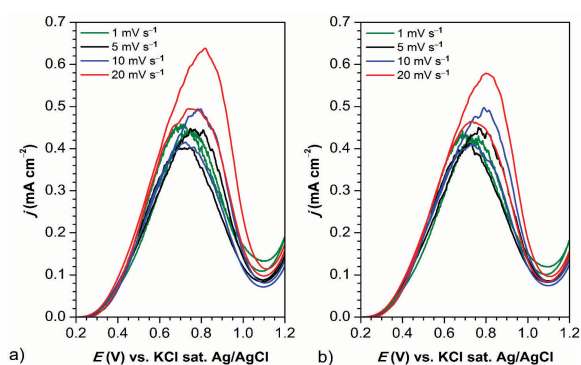
potential of the H_2O_2 catalytic response falls in the potential range from +0.60 up to +0.75. Figure 5 shows hydrodynamic chronoamperograms recorded at +0.25V in 0.1 M PBS with different increasing concentrations of H_2O_2 on: a) bare FTO electrode and b) $MnCO_3$ thin film electrode. From Figure 5 it can be seen that the chronoamperometric measurement under positive potentials showed no amperometric response of the bare FTO electrode, which confirms that the $MnCO_3$ exhibits a strong electrocatalytic activity towards H_2O_2. It was revealed that the best chronoamperometric results at potential of +0.25 V are obtained over the concentration interval from 0.09 to 1.8 mM with the sensitivity of 2.64 µA cm^{-2} mM^{-1} and R^2 = 0.999 (see Figure 6). The detection limit was found to be 10.0 µM (see Table 2) and the average response time was 3 s. The chronoamperometric measurements at potentials +0.15 V and +0.20 V resulted in significantly poorer values in terms of the detection limit, sensitivity and a concentration interval with a linear response (see Table 2). The durability tests of the $MnCO_3$ thin films as sensor for H_2O_2 showed that each sensor could be used for approximately 50 measurements. For measurements, more than 50 times, it was found that the $MnCO_3$ thin film detaches from the FTO electrode due to deficient adhesion properties of the thin film to the FTO substrate. In addition to the chronoamperometry at positive potentials, the sensor was also tested at negative potential of –0.25 V. The chronoamperometric response at –0.25 V of $MnCO_3$ thin film sensor and bare FTO are shown on Figure 7. The results showed that the amperometric response of the bare FTO layer is stronger than the response obtained when $MnCO_3$ modified FTO electrode is used. Similar results are obtained under potentials of –0.15 and –0.20 V (data not shown). $MnCO_3$ thin films deposited with thicknesses of 100 and

Figure 4. Voltammograms of FTO electrode covered with $MnCO_3$ in PBS (pH = 7.5) in the presence of H_2O_2 (c = 5.0 mM) at different scan rates. (a) Start potential: +1.20 V; 1st vertex potential: +0.20 V; 2nd vertex potential: +1.20 V. (b) Start potential: +0.20 V; 1st vertex potential: +1.20 V; 2nd vertex potential: +0.20 V.
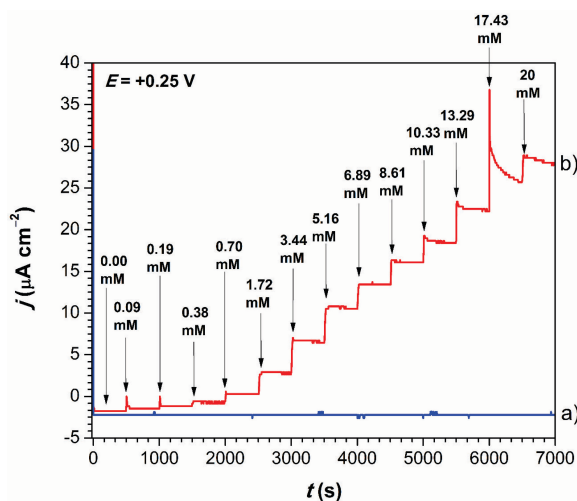

Figure 5. Chronoamperograms of: (a) Bare FTO electrode and (b) $MnCO_3$ thin film modified electrode in PBS (pH = 7.5) in the increasing concentration of H_2O_2 from 0.09 to 20.0 mM.

Table 1. Results from MnCO₃ thin film cyclic voltammetry measurements at scan rates of 1, 5, 10 and 20 mV s⁻¹ over the potential window from +0.20 to +1.20 V (see Figures 4a and 4b)

Scan rate / mV s⁻¹	Start potential / V	Peak	Peak current density / mA cm⁻²	Peak potential / V
1	+1.20	forward	+0.451	+0.705
		backward	+0.434	+0.742
	+0.20	forward	+0.424	+0.750
		backward	+0.430	+0.697
5	+1.20	forward	+0.401	+0.718
		backward	+0.443	+0.759
	+0.20	forward	+0.451	+0.764
		backward	+0.411	+0.720
10	+1.20	forward	+0.415	+0.722
		backward	+0.493	+0.781
	+0.20	forward	+0.494	+0.784
		backward	+0.411	+0.730
20	+1.20	forward	+0.494	+0.758
		backward	+0.638	+0.816
	+0.20	forward	+0.579	+0.799
		backward	+0.462	+0.751

150 nm were also examined with chronoamperometry at applied potential of +0.25 V and poor results were obtained in terms of their detection limit and sensitivity due to the low electric conductivity of the material with higher thickness (see Table S1 from Supplementary material).

Finally, the amperometic MnCO₃ thin film sensor was probed for possible interference with different important ions and compounds. The following ions have been tested as a possible interfering substances to the sensor operating under anodic conditions: Na⁺, K⁺, NO₂⁻, Cl⁻, citrate ions and D-(+)-glucose. Aqueous solutions of these substances were injected in situ as calculated aliquots in the system sequentially (one by one) after an aliquot of H₂O₂. After the injection of each substance, an aliquot of H₂O₂ is again injected in order to estimate that the sensor is still stable and functional. The amperometric response of these interfering species is negligible and comparable to the common noise at the working potential of +0.25 V (see Figure S7 from Supplementary material). The H₂PO₄⁻ and HPO₄²⁻ ions present in the PBS are also proven not to interfere significantly during the electrochemical experiments, at the same applied potential of +0.25 V (see Figure 2).
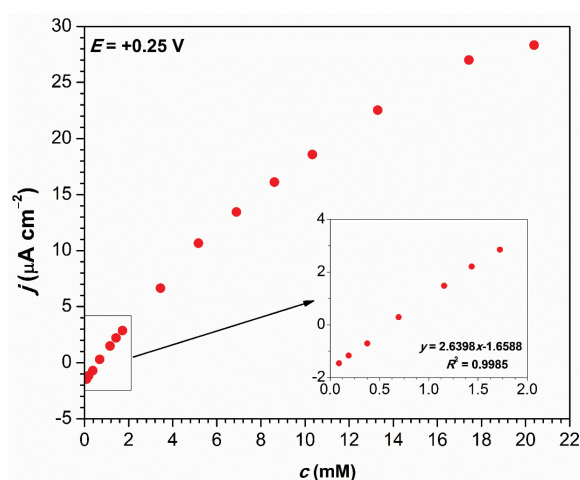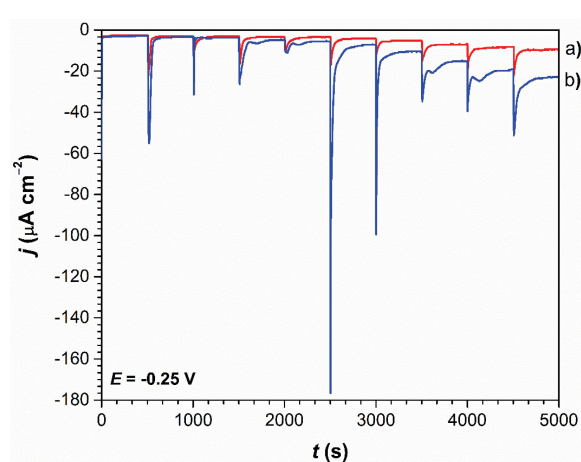

Figure 6. Current density vs. H₂O₂ concentration in the total examined range and calibration plot of the current density vs. H₂O₂ concentration over the interval from 0.09 to 1.8 mM.

Figure 7. Chronoamperograms under cathodic potential examined in PBS (pH = 7.5) in the presence of H₂O₂ with concentrations from 0.09 to 20.0 mM: (a) MnCO₃ thin film modified electrode and (b) Bare FTO electrode.

Table 2. Results from the chronoamperometry examinations of the MnCO₃ thin film modified electrodes at different applied potentials.
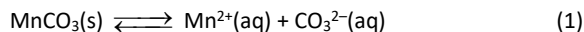
Applied potential / V	Detection limit / μM	Sensitivity / μA cm⁻² mM⁻¹	Concentration interval of linear amperometric response / mM
+0.15	no detection	no quantification	–
+0.20	351.76	0.31	0.6–7.0
+0.25	10.0	2.64	0.09–1.8[a]

[a] The sensitivity refers to the first concentration interval in which the response is linear. The maximal quantification concentration is 20 mM but with decreased sensitivity.
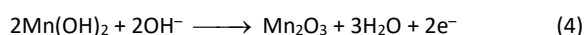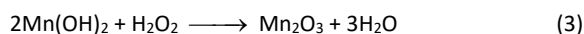
DISCUSSION

The simple chemical bath deposition method that was used to modify the FTO electrode has proven to be reliable and reproducible, allowing us to synthesize the same MnCO₃ material each time by strict time dependant thickness of the films, according to Stojkovikj *et al* (see Figure 1).[1] According to the electrochemical results from the cyclic voltammetry measurements, it may be summarized that the oxidative processes, giving rise to an anodic voltammetric tail, undergoes at potentials more positive than +1.10 V. Moreover, it is assumed that this is attributed to the different Mn species.[37,41] Figure S5 (from Supplementary material) shows typical cyclic voltammogram of FTO electrode covered with MnCO₃ thin film in PBS (pH = 7.5) in the absence of H₂O₂ and a voltammogram of bare FTO electrode, added for comparison. These cyclic voltammograms indicate that there is also an electrochemical activity in the potential window from −0.25 to +1.0 V, possibly caused by oxidation of Mn(II) into Mn(III) or Mn(IV) species involving processes further described with Equations (4) and (5). On the other hand, the working electrode modified with MnCO₃ thin film exhibits a complex electrochemical behaviour in the presence of H₂O₂, at the entire tested H₂O₂ concentrations, i.e. from 0.05 to 5.0 mM (see Figure 3). The voltammograms feature the same, uncatalized cathodic processes as at the bare FTO electrode at potentials more negative than −0.25 V. However, in the anodic part of the voltammograms, at potentials more positive than +0.25 V, a new, broad anodic peak is observed due to catalytic oxidation of H₂O₂ at MnCO₃ thin film electrode. Interestingly, the latter anodic peak is formed in both forward and reverse potential scans. Hence, this phenomenon is being more strongly emphasized at concentrations of H₂O₂ above 0.5 (see Figure 3). Such peculiar voltammetric behaviour is considered that occurs as a consequence of the intensive catalytic processes between the polyvalent manganese species and H₂O₂.[20,44,48] Concentrations of H₂O₂ above 30 mM caused formation of ill-shaped cyclic voltammograms (Figure S6 from Supplementary material) due to the process of dissolving of the MnCO₃ thin film in the electrolyte, revealing the upper limit of the MnCO₃ thin film electrode

considered as an electrochemical sensor. In a general context, the electrochemical transformation of H₂O₂ at the MnCO₃ thin film electrode must be affected by mass transfer phenomena of H₂O₂, as well as by a possible intercalation processes related to K⁺ ions from the electrolyte solution into the thin film structure.[8,55,58] The electrocatalytic mechanism could be however rationalized by considering several known chemical and electrochemical transformations of manganese species.[44,48,53,58] Based on that a plausible sensing mechanism is proposed and discussed for the MnCO₃ thin film H₂O₂ sensor. First, the process of a slight dissolving and dissociation of MnCO₃ in the vicinity of the thin film modified electrode surface has to be considered [see Eq. (1)]. This reaction is simultaneously accompanied with formation of Mn(OH)₂ in the slightly alkaline medium at pH = 7.5 [see Eq. (2)].

$$MnCO_3(s) \rightleftharpoons Mn^{2+}(aq) + CO_3^{2-}(aq) \qquad (1)$$

$$Mn^{2+}(aq) + 2OH^-(aq) \rightleftharpoons Mn(OH)_2(s) \qquad (2)$$

It is considered that the Mn(OH)₂ in presence of H₂O₂ is chemically and/or electrochemically oxidized into Mn₂O₃, [see Eqs. (3) and (4), respectively]. This assumption is supported by the fact that Mn₂O₃ is thermodynamically the most stable manganese form at pH ≥ 7.[44,48]

$$2Mn(OH)_2 + H_2O_2 \longrightarrow Mn_2O_3 + 3H_2O \qquad (3)$$

$$2Mn(OH)_2 + 2OH^- \longrightarrow Mn_2O_3 + 3H_2O + 2e^- \qquad (4)$$

The electrochemical oxidation of Mn(III) species into MnO₂ is another possible process taking part in the sensing mechanism of H₂O₂ and it is described with Eq. (5).[12,44,48,58]

$$Mn_2O_3 + 2OH^- \longrightarrow 2MnO_2 + H_2O + 2e^- \qquad (5)$$
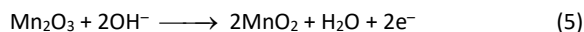
It is considered that MnO₂, as a product of the electrode reaction is involved into chemical redox reactions in presence of H₂O₂ [see Eqs. (6) and (7)] to form Mn(II) and Mn(III) species. Thus, MnO₂ acts as a redox catalysts for electrocatalytic transformation of H₂O₂. The proposed reaction [Eq. (6)] is in agreement with the work of Luo *et al*.[58] They showed that MnO₂ nanoparticles directly oxidize H₂O₂ to form O₂ and Mn(II) species. It is considered that the same oxidation process of H₂O₂ is taking place even when Mn(IV) species are reduced in the diffusion layer to Mn(III)

species [see Eq. (7)][53], thereby taking into account that Mn(III) species are thermodynamically the most stable species at pH ≥ 7.[44,48]

$$MnO_2 + H_2O_2 \longrightarrow Mn(OH)_2 + O_2 \qquad (6)$$

$$2MnO_2 + H_2O_2 \longrightarrow Mn_2O_3 + H_2O + O_2 \qquad (7)$$
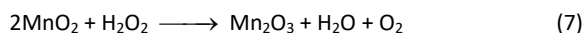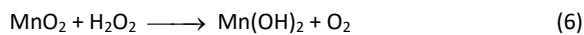
Therefore, the electrode reaction [Eq. (5)], coupled with the follow–up redox reactions [Eq. (6)] and [Eq. (7)], complete the scheme of a typical catalytic, regenerative electrode mechanism of the EC' type, where Mn(IV)/Mn(III) and Mn(IV)/Mn(II) redox couples serve as redox mediators, shuttling electrons between H$_2$O$_2$ and the electrode. Our findings are in agreement with the report of Cui *et al.*[12] They showed that MnO$_2$/RGE/P25 nanocomposites exhibit a broad oxidation peak at +0.71 V vs. SCE in a PBS (pH = 8, *c* = 0.1 M) in presence of 0.1 mM H$_2$O$_2$ and they have assigned this oxidation to the electrochemical oxidation of Mn(II) and Mn(III) species, formed in analogous reactions as described with Eqs. (6) and (7). In all experiments, the anodic peak is formed in both forward and reverse potential scans, the peak current and potential values are listed in Table 1. The peak potential of the anodic peaks is slightly shifted towards more positive potentials by increasing the scan rate from 1 to 20 mV s^{-1} (see Table 1 and Figure 4). Evidently, at a low scan rate and a large H$_2$O$_2$ concentration the electrocatalytic sensing mechanism proceeds at significant rate, maintaining steady–state conditions at the electrode surface. Thus, causing the voltammetric curve to follow virtually an identical trace regardless of the starting potential. At very low scan rate (1 mV s^{-1}), the peak currents are almost identical for the forward and reverse anodic peaks (Δj_p = 6 μA cm^{-2}) reflecting a truly steady-state conditions, whereas at 20 mV s^{-1}, the peak current difference is becoming significant (Δj_p = 117 μA cm^{-2}). It is assumed that maybe this is due to the drift from equilibrium conditions in the course of the voltammetric experiment (cf. Table 1 and Figure 4) but on the other hand if we consider deeper explanation, we could presume that there are some non-Faradaic i.e. capacitive processes occurring at higher scan rates in the electric double layer. The measured total current presents a sum of the Faradaic current (electrode reaction) and the capacitive current (double layer charging): $i = i_f + i_c$. The capacitive current is dependent from the scan rate i.e. $i_c = Cd(dE/dt)$, where *Cd* is the double layer capacitance and dE/dt is the scan rate. In conclusion, the current increase and thus significant difference in the peak current values is a consequence to the increase in the capacitive current as the scan rate increases, and this behaviour is only obvious at the highest measured scan rate of 20 mV/s.

The peak-like shape of the response is a consequence of losing the redox mediator species (i.e. Mn(III) and Mn(IV) forms) at potentials more positive than +0.75 V through further electrochemical oxidation to higher–valent manganese species that are catalytically inactive toward H$_2$O$_2$ oxidation. This is supported by the appearance of the strong anodic current in a form of a voltammetric tail at the positive potential side of the voltammogram (cf. Figure 3). The voltammograms depicted on Figure 3 shows that the peak is rather broad and the increase of the current commences even at potential close to +0.20 V. Therefore, the potential of +0.25 V was selected as an optimal potential for the chronoamperometric experiments as it provides sufficient sensitivity and as well minimizes the possible interferences of concurrent, concomitant oxidative processes.

The results of the chronoamperometric measurements, represented as a dependence of the current density *vs.* concentration, can be approximated with a linear regression line described with Eq. (8).

$$j/\mu A\ cm^{-2} = a/\mu A\ cm^{-2} + b/\mu A\ cm^{-2}\ mM^{-1} \cdot c/mM \qquad (8)$$

where the slope $-b$/μA cm^{-2} mM^{-1} represents the sensitivity of the sensor.

On the other hand, the total amperometric dependence in the whole examined H$_2$O$_2$ concentration interval (0.09 – 20 mM) actually represents a curved line (see Figure 6). It is considered that the reason for this behaviour arises from the complexity of the electrode mechanism, such as possible complications due to H$_2$O$_2$ adsorption, and/or due to the influence of the ohmic drop effect at large H$_2$O$_2$ concentrations and corresponding high current density.

Regarding the processes that are taking place when the working electrode has a function of a cathode, it is assumed that are running only through a reduction of H$_2$O$_2$ without involving Mn(II, III and IV) species present in the diffusion layer. This assumption is based on the conclusion after comparing the voltammograms shown in Figures 2 and 3. Since the response of H$_2$O$_2$ at negative potentials is virtually identical at bare and MnCO$_3$ modified FTO electrode, one can assume that the reduction of H$_2$O$_2$ occurs directly at FTO electrode surface, excluding any electrocatalytic mechanism involving manganese species. Moreover, the bare FTO electrode exhibits a slightly higher sensitivity towards H$_2$O$_2$ compared to MnCO$_3$ modified electrode (see Figure 7). However, the amperometric response on the bare FTO electrode towards H$_2$O$_2$ is less reproducible than on the electrode modified with MnCO$_3$ thin film.

CONCLUSIONS

In this paper a novel and simple approach to design a non–enzymatic amperometric sensor for H_2O_2 quantification based on $MnCO_3$ thin film electrode, has been presented. The films were prepared with a thickness of 75 nm on a surface of FTO coated glass substrates using a simple chemical deposition technique. The methods that were used for characterization of the sensors were XRD, cyclic voltammetry and hydrodynamic chronoamperometry. The XRD analysis confirmed the qualitative chemical composition of the deposited thin films that corresponds to well crystalized rhodochrosite phase $MnCO_3$. Cyclic voltammetry examinations showed that the sensing mechanism consists of catalytic, where polyvalent manganese species - Mn (II, III and IV), serve as redox mediators, transporting electrons between H_2O_2 and the electrode. Hydrodynamic chronoamperometry measurements were carried out in a wide H_2O_2 concentration interval from 0.09 to 20 mM, by applying both anodic and cathodic potentials of 0.15, 0.20 and 0.25 V. The best results are obtained at an anodic potential of +0.25 V and concentration range of H_2O_2 from 0.09 up to 1.8 mM. The lowest obtained detection limit at this potential is 10 µM with sensitivity of 2.64 µA cm^{-2} mM^{-1} and a linear calibration plot, R^2 = 0.999. When the sensor is tested in a wider concentration interval of H_2O_2 (from 0.09 to 20 mM) the linearity of the calibration plot decreases. The selectivity of the sensor was tested in presence of some electroactive species and their amperometric response is negligible and comparable to the common noise at the working potential of +0.25 V. The durability tests of the $MnCO_3$ thin films as sensor for H_2O_2 showed that each sensor could be used for approximately 50 measurements. Unfortunately, this sensor cannot be applied for detection and quantification of H_2O_2 in biological systems due to the higher detection limit, but we are encouraging its application in the chemical, pharmaceutical, and food and beverage industry.

Conflicts of interest statement. This research did not receive any specific grant from funding agencies in the public, commercial, or not-for-profit sectors. The authors declare that they have no conflict of interest.

Supplementary Information. Supporting information to the paper is attached to the electronic version of the article at: https://doi.org/10.5562/cca3424.

REFERENCES

[1] S. Stojkovikj, M. Najdoski, V. Koleva, S. Demiri, *J. Phys. Chem. Solids* **2013**, *74*, 1433.

[2] E. S. M. Seo, W. K. Yoshito, V. Ussui, D. R. R. Lazar, S. R. H. de Mello Castanho, J. O. A. Paschoal, *Mat. Res.* **2004**, *7*, 215.

[3] P. V. Vardhan, M. B. Idris, S. Manikandan, K. S. Rajan, S. Devaraj, *J. Solid State Electrochem*. **2018**, *22*, 1795.

[4] P. V. Vardhan, S. Sridhar, S. R. Sivakkumar, U. K. Mudali, S. Devaraj, *J. Nanosci. Nanotechnol.* **2018**, *18*, 2775.

[5] P. V. Vardhan, M. B. Idris, H. Y. Liu, S. R. Sivakkumar, P. Balaya, S. Devaraj, *J. Electrochem. Soc.* **2018**, *165*, A1865.

[6] P. V. Vardhan, M. B. Idris, V. Ramanathan, S. Devaraj, *ChemistrySelect* **2018**, 3, 6775.

[7] M. Jana, P. Samanta, N. C. Murmuab, T. Kuila, *J. Mater. Chem. A* **2017**, *5*, 12863.

[8] W. Xu, J. Liu, M. Wang, L. Chen, X. Wang, C. Hu, *Anal. Chim. Acta* **2016**, *913*, 128.

[9] J. H. Lee, H. G. Hong, *J. Appl. Electrochem*. *45*:1153.

[10] L. Luo, F. Li, L. Zhu, Z. Zhang, Y. Ding, D. Deng, *Electrochim. Acta*. **2012**, *77*, 179.

[11] G. Scandurra, A. Arena, C. Ciofi, G. Saitta, *Sensors* **2013**, *13*, 3878.

[12] S. Cui, Y. Li, D. Deng, L. Zeng, X. Yan, J. Qian, L. Luo, *RCS Adv*. **2016**, *6*, 2632.

[13] Chen W, Cai S, Ren QQ, Wen W, Zhao YD, *Analyst* **2012**, *137*, 49.

[14] B. Thirumalraj, D. H. Zhao, S. M. Chen, S. Palanisamy, *J. Colloid. Interface. Sci*. **2016**, *470*, 117.

[15] L. Zhang, Z. Fang, Y. Ni, G. Zhao, *Int. J. Electrochem. Sci*. **2009**, *4*, 407.

[16] M. Asif, A. Aziz, A.Q. Dao, A. Hakeem, H. Wang, S. Dong, G. Zhang, F. Xiao, H. Liu, *Anal. Chim. Acta* **2015**, *898*, 34.

[17] M. Bozem, P. Knapp, V. Mirčeski, E.J. Slowik, I. Bogeski, R. Kappl, C. Heinemann, M. Hoth, *Antioxid. Redox. Signal.* **2017**.

[18] A. Boveris, E. Cadenas, *IUBMB Life* **2000**, *50*, 245.

[19] M. Giorgio, M. Trinei, E. Migliaccio, P.G. Pelicci, *Nat. Rev. Mol. Cell. Biol*. **2007**, *8*, 722.

[20] S. Dong, J. Xi, Y. Wu, H. Liu, C. Fu, H. Liu, F. Xiao, *Anal. Chim. Acta* **2015**, *853*, 200.

[21] E. W. Miller, B. C. Dickinson, C. J. Chang, *Proc. Natl. Acad. Sci*. **2010**, *7*, 15681.

[22] W. C. Schumb, C. N. Satterfield, R. L. Wentworth, *Hydrogen Peroxide*, Reinhold Publishing Corp., New York, **1955**.

[23] S. Hanaoka, J. M. Lin, M. Yamada, *Anal. Chim. Acta* **2001**, *426*, 57.

[24] Y. Hu, Z. Zhang, C. Yang, *Anal. Chim. Acta* **2007**, *601*, 95.

[25] Y. Shiang, C. Huang, H. Chang, *Chem. Commun*. **2009**, *23*, 3437.

[26] O. S. Wolfbeis, A. Dürkop, M. Wu, Z. Lin, *Angew. Chem*. **2002,** *41*, 4495.

[27] E. Fernandes, A. Gomes, J. L. F. C. Lima, *J. Biochem. Biophys. Methods* **2005**, *65*, 45.

[28] R. Zhang, S. He, C. Zhang, W. Chen, *J. Mater. Chem. B* **2015**, *3*, 4146.

[29] M. E. Abbas, W. Luo, L. Zhu, J. Zou, H. Tang, *Food Chem.* **2010**, *120*, 327.

[30] R. F. Nogueira, M. C. Oliveira, W. C. Paterlini, *Talanta* **2005**, *66*, 86.

[31] A. Zaribafan, K. Haghbeen, M. Fazli, A. Akhonda, *Environmental Studies of Persian Gulf* **2014**, *1*, 93.

[32] K. Sunil, B. Narayana, *Bull. Environ. Contam. Toxicol.* **2008**, *81*, 422.

[33] U. Pinkernell, S. Effkemann, U. Karst, *Anal. Chem*. **1997**, *69*, 3623.

[34] R. Ramachandran, S. M. Chen, G. Gnana kumar, P. Gajendran, A. Xavier, N. B. Devi, *Int. J. Electrochem. Sci.* **2016**, *11*, 1247.

[35] L. Wang, E. Wang, *Electrochem. Commun*. **2004**, *6*, 225.

[36] Y. Wang, Y. Hasebe, *Materials* **2014**, *7*, 1142.

[37] V. Ganesh, A. Muthurasu, *Journal of Physics: Conference Series.* **2012**.

[38] A. Morales, F. Céspedes, J. Mũnoz, E. Martínez-Fábregas, S. Alegret, *Anal. Chim. Acta* **1996**, *332*, 131.

[39] S. Xu, B. Peng, X. Z. Han, *Biosens. Bioelectron*. **2007**, *22*, 1807.

[40] L. Bai, R. Yuan, Y. Chai, Y. Yuan, L. Mao, Y. Zhuo, *Analyst* **2011**, *136*, 1840.

[41] H. Li, Y. Li, S. Wang, *Cryst. Eng. Comm.* **2015**, *17*, 2368.

[42] S. He, B. Zhang, M. Liu, W. Chen, *RSC Adv.* **2014**, *4*, 49315.

[43] P. Zhang, D. Guo, Q. Li, *Mater. Lett*. **2014**, *125*, 202.

[44] B. Xu, M. L. Ye, Y. X. Yu, W. D. Zhang, *Anal. Chim. Acta* **2010**, *674*, 20.

[45] W. Bai, J. Zheng, Q. Sheng, *Electroanal.* **2013***, 25*, 2305.

[46] L. Wang, M. Deng, G. Ding, S. Chen, F. Xu, *Electrochim. Acta* **2013**, *114*, 416.

[47] S. Thiagarajan, T. H. Tsai, S. M. Chen, *Int. J. Electrochem. Sci.* **2011**, *6*, 2235.

[48] Y. H. Bai, Y. Du, J. J. Xu, H. Y. Chen, *Electrochem. Commun*. **2007**, 9, 2611.

[49] X. Xiao, Y. Song, H. Liu, M. Xie, H. Hou, L. Wang, Z. Li, *J. Matter. Sci.* **2013**, *48*, 4843.

[50] S. Liu, L. Li, Q. Hao, X. Yin, M. Zhang, Q. Li, L. Chen, T. Wang, *Talanta* **2010***, 81*, 727.

[51] A. J. Wang, P. P. Zhang, Y. F. Li, J. J. Feng, W. J. Dong, X. Y. Liu, *Microchim. Acta* **2011**, *175*, 31.

[52] Y. Han, J. Zheng, S. Dong, *Electrochim. Acta* **2013**, *90*, 35.

[53] Y. Pan, Z. Hou, W. Yi, W. Zhu, F. Zeng, Y. N. Liu, *Talanta* **2015**, *141*, 86.

[54] M. R. Mahmoudian, Y. Alias, W. J. Basirun, P. M. Woi, M. Sookhakian, *Sens. Actuator B–Chem.* **2014**, *201*, 526.

[55] A. Salimi, M. Mahdioun, A. Noorbakhsh, A. Abdolmaleki, R. Ghavami, *Electrochim. Acta* **2011**, *56*, 3387.

[56] D. Ye, X. Li, G. Liang, J. Luo, X. Zhang, S. Zhang, H. Chen, J. Kong, *Electrochim. Acta* **2013**, *109*, 195.

[57] L. Li, Z. Du, S. Liu, Q. Hao, Y. Wang, Q. Li, T. Wang, *Talanta* **2010**, *82*, 1637.

[58] X. L. Luo, J. J. Xu, W. Zhao, H. Y. Chen, *Biosens. Bioelectron*. **2004**, *19*, 1295.